

## Using Primary Instability Analysis for Determination of Apparent Liquid Viscosity at Jet Breakup Atomizing Non-Newtonian Fluids

Sänger Alexander\*<sup>1</sup>, Tobias Jakobs<sup>1</sup>, Thomas Kolb<sup>1,2</sup>

Karlsruhe Institute of Technology (KIT), Karlsruhe, D

<sup>1</sup>Institute for Technical Chemistry, KIT Campus North

<sup>2</sup>Engler-Bunte-Institute, KIT Campus South

\*Corresponding author: alexander.saenger@kit.edu

### Abstract

Motivated by the atomization of rheological complex fluids in industrial application like entrained flow gasification (EFG) or combustion processes, the research work of the present study deals with atomization of non-Newtonian fluids (NN) with shear-thinning flow behavior. The focus is on a new experimental approach for estimation of the apparent shear viscosity  $\eta_{liq}^*$  at the jet breakup process during atomization of NN-fluids using an external mixing twin-fluid atomizer. This experimental approach is based on the viscosity dependence of the passage frequency  $f_{prim}$  of shear instability (Kelvin-Helmholtz type) in the near nozzle region. Knowing  $f_{prim}$  as function of liquid viscosity, the apparent viscosity  $\eta_{liq}^*$  can be deduced from measuring  $f_{prim,NN}$  during atomization of NN-fluids. For the investigated NN-fluid it was shown by the use of high-speed images that the liquid viscosity must be lowered due to shear between gas and liquid. In fact, this was validated by determination of  $\eta_{liq}^*$  using the new method. In addition, a first attempt to correlate spray quality with an extended Oh number ( $D_{32} \propto (Oh^*)^x$ ) by the use of  $\eta_{liq}^*$  determined with the new method was successful. Increased accuracy was achieved compared to the definition of Oh\* typically using viscosity values at low  $\eta_{liq,0} = \eta_{liq}(\dot{\gamma} \rightarrow 0)$  or high  $\eta_{liq,\infty} = \eta_{liq}(\dot{\gamma} \rightarrow \infty)$  shear rates  $\dot{\gamma}$ .

### Introduction

Liquid and suspension fuels are widely used as feedstock in technical combustion and gasification processes for energy conversion. In general, the fuel has to be dispersed with an atomizer into a fine spray to achieve a good performance of the systems, i.e. high efficiency and minimum emission of exhaust pollutants. The conversion of low-grade fossil or biogenic energy resources (e.g. low rank coal, biomass) to a high quality chemical energy carrier (synthesis gas) in a high pressure entrained flow gasifier (EFG) is one option for an efficient use of low grade energy resources, refer to Higman and van der Burgt [1].

The syngas produced may be converted into high value products like methanol, methane (substitute natural gas, SNG) or liquid fuels (biomass to liquid, BtL / coal to liquid, CtL) and it may also be fired in a gas turbine of a combined cycle power plant to produce electricity. The operation of an entrained flow gasifier aims for complete fuel conversion within the reaction chamber at a given temperature and residence time. For liquid or slurry fed EFG systems the fuel conversion efficiency depends strongly on the atomization process. Droplet size distribution and spray angle generated by the atomizer considerably influence the flow pattern, concentration and temperature distribution in the burner near field and thus the fuel conversion characteristics. For the design and process optimization of technical gasifiers, a fundamental knowledge and understanding of the atomization process (e.g. jet disintegration process, spray characteristics) is mandatory. In this context, spray investigations for combustion application, i.e. gas turbines, fuel injection (gasoline/diesel engines) or rocket propulsion, have been conducted over the years for a wide range of operating conditions, different types of nozzles and typically low viscous liquids ( $\eta_{liq} < 20 \text{ mPa s}$ ). Nevertheless, little has been investigated and published concerning atomization under conditions relevant for EFG. The nozzle type of interest for liquid and suspension fed EFG are commonly known as gas-assisted atomizers. Concerning the possible risk of abrasion and clogging as well as coking due to the high process temperatures, preferably external mixing gas-assisted atomizers are used (Hede et al. [2]). Twin-fluid atomization for EFG faces several challenges arising from the specific technical operating conditions. Typically, the systems are operated with gasifying high viscous liquid or suspension fuels featuring viscosities up to  $\eta_{liq} = 1000 \text{ mPa s}$  and complex rheological behavior (i.e. shear-thinning flow behavior). Additionally, the atomization of such fuels is performed at elevated ambient pressure (up to 80 bar (abs)) to account for the demand of subsequent process steps (Kolb and Eberhard [3]). Furthermore, to achieve a high efficiency of the gasification process the gasification agent oxygen also serves as atomization agent. Based on the required stoichiometry of the gasification reaction there is only a limited amount of gasification agent and therefore atomization agent available (see Sanger et al.[4]).

Especially the influence of rheology on atomization must be considered because of the pronounced influence of dynamic viscosity and non-Newtonian flow behavior of the fuels on the spray quality. Primary breakup

morphology and spray quality (drop size distribution) of a spray generated by a twin-fluid atomizer is typically described by the use of dimensionless parameters like Weber number ( $We$ ), gas-to-liquid ratio (GLR), and Ohnesorge number ( $Oh$ ). The Weber number (see. Eq. (1)) describes the ratio of aerodynamic forces to surface tension forces. Depending on definition of  $L_c$ , the Weber number describes jet breakup  $i = \text{aero}$  ( $L_c = D_{liq}$ ) or single droplet disintegration  $i = \text{dr}$  ( $L_c = D_{dr}$ ), where  $D_{liq}$  defines the diameter of the undisturbed liquid jet and  $D_{dr}$  the diameter of a single drop. Further  $v_{rel}$  defines the relative velocity between gas  $v_{gas}$  and liquid phase  $v_{liq}$ ,  $\rho_{gas}$  the density of the gas and  $\sigma$  is the surface tension of the atomized liquid.

$$We_i = \frac{v_{rel}^2 \rho_{gas} L_c}{\sigma} \quad (1)$$

In gas-assisted atomization the ratio of gas  $\dot{m}_{gas}$  to liquid  $\dot{m}_{liq}$  mass flow is defined as

$$GLR = \frac{\dot{m}_{gas}}{\dot{m}_{liq}} \quad (2)$$

which elucidates for constant nozzle geometry (fixed aspect ratio) the relevance of gas velocity. Drop size typically decreases with increasing GLR, e.g. Hede et al. [2].

The influence of liquid dynamic viscosity  $\eta_{liq}$  on spray quality or breakup morphology (i.e. primary breakup and secondary breakup) in case of Newtonian liquids ( $\eta_{liq} \neq f(\dot{\gamma})$ ) is described by the Ohnesorge number

$$Oh = \frac{\eta_{liq}}{(\sigma \rho_{liq} D_{liq})^{0.5}} \quad (3)$$

which relates viscous forces to surface tension forces. The parameter  $\rho_{liq}$  corresponds to the liquid density. For external mixing twin-fluid atomizers (EMTFA) Kim and Marshall [5], Mulhem et al. [6], Schmelz and Walzel [7] and Aliseda et al. [8] presented spray investigations for various N-liquids with viscosities in the range of  $\eta_{liq} \approx 1 - 100$  mPa s. All authors found an increase of drop size (typically expressed by characteristic diameters e.g. Sauter mean diameter  $D_{32}$ ) for increasing  $\eta_{liq}$  respectively  $Oh$ . This effect is more pronounced for low GLR ratios compared to higher values. In addition, Sanger et al. [4] investigated the influence of  $\eta_{liq}$  for an extended range of viscosities (up to  $\eta_{liq} = 400$  mPa s). This investigation revealed an unexpected influence of  $\eta_{liq}$  on spray quality, caused by to different primary jet instabilities, for viscosities significantly larger compared to the typically in literature (EMTFA) examined viscosity ranges. In contrast to Newtonian liquids, typical fuels for EFG show a non-Newtonian (NN) shear-thinning flow behavior ( $\eta_{liq} = f(\dot{\gamma})$ ) which means that viscosity depends on shear rate  $\dot{\gamma}$ . In this case, the influence of viscosity on atomization behavior cannot be described by the use of the common  $Oh$  number due to the dependence of dynamic viscosity on shear stress for NN-fluids which is relevant at the nozzle exit where the gas jet interacts with the liquid. Thus, the apparent viscosity  $\eta_{liq}^*$  as a function of operational parameters (e.g.  $v_{rel}$ ) is needed to determine an extended  $Oh^*$  number

$$Oh^* = \frac{\eta_{liq}^* = \eta_{liq}(\dot{\gamma})}{(\sigma \rho_{liq} D_{liq})^{0.5}} \quad (4)$$

Only few investigations on atomization of NN-liquids using EMTFA are given in literature. Most of them are related to industrial processes in which NN-fluids (typical shear-thinning) are used (i.e. slurry combustion, rocket engine combustion and suspension spray drying). The aim of these studies is to determine how NN-fluid rheology affects spray processes like primary and secondary atomization. A particular challenge is to integrate fluid rheology ( $\eta_{liq} = f(\dot{\gamma})$ ) into the model based description of the spray process (e.g.  $D_{32} \propto Oh^*$ ). In other words, to estimate reasonable accurate the shear rate  $\dot{\gamma}$  and therefore the apparent shear viscosity  $\eta_{liq}^*$  relevant for jet breakup during atomization of NN-fluids.

Mansour and Chigier [9] investigated atomization of viscous NN-liquids (xanthan gum and polyacrylamide) using EMTFA. The authors showed experimentally that spray quality is closely related to the apparent viscosity at shear rates to infinity  $\eta_{liq}^* = \eta_{liq}(\dot{\gamma} \rightarrow \infty)$  for shear rates in the liquid injection tube  $\dot{\gamma}_{inj} = 8 v_{liq}/D_{liq}$  larger than  $3600$  s<sup>-1</sup>. Vice versa for  $\dot{\gamma}_{inj} \leq 3600$  s<sup>-1</sup> the apparent viscosity is intermediate between  $\eta_{liq} = \eta_{liq}(\dot{\gamma} \rightarrow 0)$  and  $\eta_{liq}^* = \eta_{liq}(\dot{\gamma} \rightarrow \infty)$ . For computation of the  $Oh^*$  number the apparent viscosity was determined at  $\dot{\gamma} \approx 20000$  s<sup>-1</sup> using a capillary viscometer. Aliseda et al. [8] investigated atomization of NN-fluids for tablet coating process both theoretically and experimentally. Three commercially available water based suspensions with shear-thinning flow behavior were investigated. Concerning the determination of  $\eta_{liq}^* = f(\dot{\gamma})$  the authors refer to the approach proposed by Mansour and Chigier [9]. Interestingly,  $\eta_{liq}^* = \eta_{liq}(\dot{\gamma} \rightarrow \infty)$  was determined at a value of  $\dot{\gamma} = 225$  s<sup>-1</sup> due to the maximum shear rate data available using a cone and plate viscometer. Gillberg et al. [10] studied the

atomization of shear-thinning coal-water suspensions using EMTFA. The authors defined the apparent viscosity arbitrarily at the maximum adjustable shear rate of  $\dot{\gamma} = 450 \text{ s}^{-1}$ . In contrast to the previous studies Zhao et al. [11] suggest expressing the shear rate according to  $\dot{\gamma} = \varphi(v_{gas} - v_{liq})D_{liq}^{-1}$ . Combining this equation with a common power law fluid equation (e.g. Herschel-Bulkley model) enables calculation of apparent liquid viscosity  $\eta_{liq}^*$ . The constant  $\varphi$  is determined experimentally. For the range of parameters investigated ( $v_{liq} = 0.21 - 5.80 \text{ m s}^{-1}$ ;  $v_{gas} = 0 - 160 \text{ m s}^{-1}$ ;  $D_{liq} = 5.1 \text{ mm}/9.01 \text{ mm}$ )  $\varphi = 3.2 \cdot 10^{-4}$  and therefore the maximum shear rates ( $\dot{\gamma}_{max} = 4.3 - 7.8 \text{ s}^{-1}$ ) are significantly lower compared to the values reported by Aliseda et al. [8] and Mansour and Chigier [9]. In the investigations of Mulhem et al. [6] (twin-fluid atomization of viscous NN suspensions) and Maurer [12] (twin-fluid atomization of NN printing ink) the apparent viscosity was determined in contrast to the authors mentioned above at very low shear rates  $\eta_{liq}^* = \eta_{liq}(\dot{\gamma} \rightarrow 0)$ . Investigations on NN-fluids using internal mixing twin-fluid atomizer as effervescent atomizer (e.g. Buckner and Sojka [13]) or other atomizer concepts (e.g. Kampen et al. [14]) are not explicitly considered in this report. Due to the contradictory approaches for integration of shear-thinning flow behavior of NN-fluids into the description of atomization process (i.e. primary jet breakup, spray quality  $D_{32} \propto (Oh^*)^x$ ) using EMTFA the research work of the present study is focused on a new experimental approach to estimate the apparent liquid shear viscosity  $\eta_{liq}^*$  relevant for the jet breakup process during atomization of a NN-fluid by a high-speed gas jet.

### Experimental description

The experimental setup used in the present work consists of an atmospheric spray test rig (ATMO), a laser diffraction spray particle analyser (LDS) and a high-speed camera (HG-Cam) which operates in backlight mode for spray visualization. An EMTFA was used for atomization of several pure liquids and suspensions with Newtonian and non-Newtonian flow behavior.

The spray test rig ATMO is schematically shown in Figure 1(a). An atomizer is mounted on the twin-fluid lance which is supplied with working fluids from a tempered and stirred tank using a low pulsation gear pump. In contrast to a typical pump for viscous liquids/suspensions (e.g. membrane pump), this fluid supply enables us to provide a fluid flow with minimum pulsation. This is necessary to avoid disturbances of the liquid jet (surface waves, shocks) as described by Maier et al. [15]. Liquid mass flow can be controlled with a mass flow controller (Coriolis principle) in the range of  $\dot{m}_{liq} = 1 - 20 \text{ kg h}^{-1}$ . The compressed air is also fed to the top of the lance. The air mass flow is controlled by a mass flow controller (hot wire principle) and can be varied in the range of  $\dot{m}_{gas} = 1 - 20 \text{ kg h}^{-1}$ . The atomized liquid is collected in a container. A honeycomb structure at the inlet of the container serves as flow conditioner and prevents recirculation of small droplets.

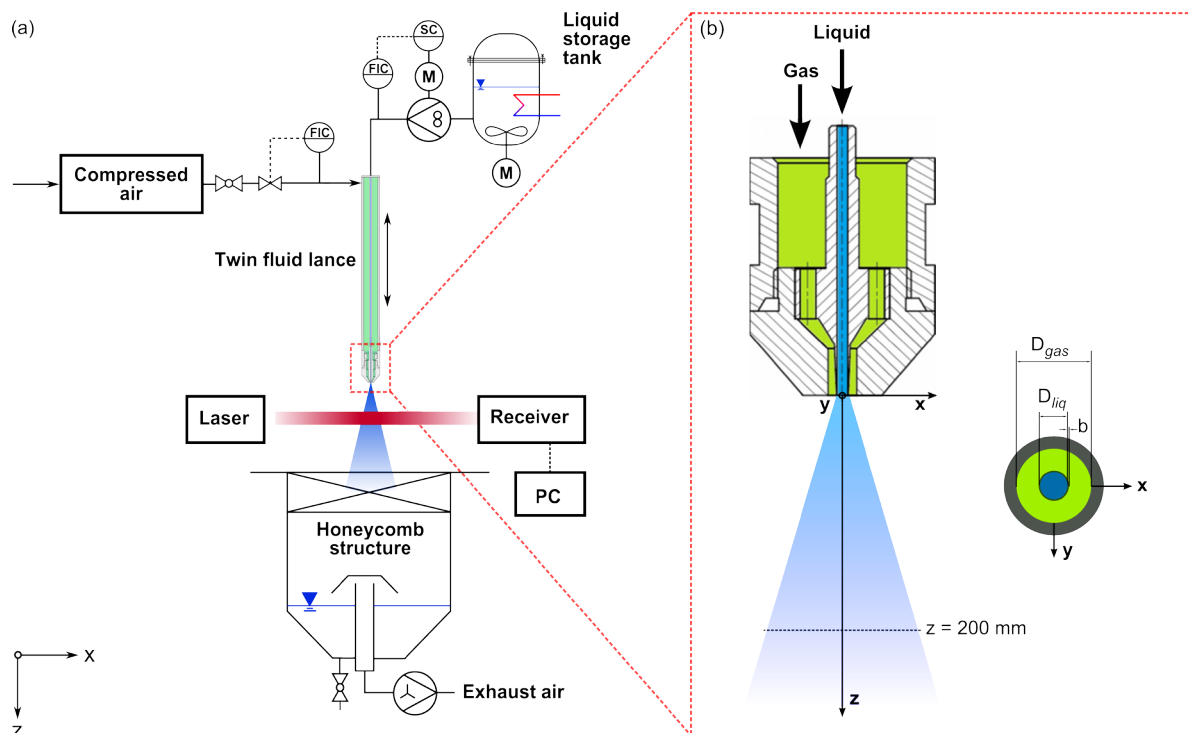


Figure 1. Schematic of the experimental setup – atmospheric spray test rig (ATMO)

Experiments were carried out using the external mixing twin-fluid atomizer shown in Figure 1(b). The liquid is injected into a circular tube ( $D_{liq} = 2$  mm) at the centerline of the atomizer. The liquid jet is surrounded by a coaxial gas stream. For better understanding of the atomization process a simple nozzle geometry (air and liquid are parallel discharged in axial direction) was chosen. Additionally, the influence of a pre-filming surface was minimized by reducing the separating wall thickness to  $b = 0.1$  mm.

For this investigation eight different fluids with significant different rheology were utilized. As Newtonian liquids six different glycerol/water-mixtures with different dynamic viscosities  $\eta_{liq}$  were used. Glycerol of 99.5 wt.% purity ( $\eta_{liq} = 1484$  mPa s at 20 °C) was diluted with pure water to obtain the desired dynamic viscosity in the range of 50 mPa s up to 400 mPa s. The physical properties of the investigated N-fluids are given in Table 1 and were measured at 20 °C and ambient pressure  $p_a = 1.013$  bar (abs).

**Table 1.** Physical properties of Newtonian (N) model fluids (at 20 °C and 1.013 bar (abs))

	$\eta_{liq}$ mPa s	$\rho_{liq}$ kg m <sup>-3</sup>	$\sigma$ mN m <sup>-1</sup>	$\mathbf{n} = n + iA$ -	Oh -
78.5 wt.% glycerol-water	50	1204	65.6	1.441 + i0	0.1258
84.5 wt.% glycerol-water	100	1220	64.9	1.450 + i0	0.2513
89.5 wt.% glycerol-water	200	1233	64.2	1.458 + i0	0.5027
92.1 wt.% glycerol-water	300	1240	63.8	1.461 + i0	0.7542
93.8 wt.% glycerol-water	400	1244	63.6	1.464 + i0	1.0056

Glycerol/water-mixtures are particularly suitable as model fluids. Due to negligibly small variation of  $\sigma$  and  $\rho_{liq}$  in various glycerol/water-mixtures, the influence of dynamic viscosity can be analyzed isolated from the influence of other liquid properties. In addition to the N-liquids, two non-Newtonian fluids were used as well. For isolated investigation of shear-thinning flow behavior as a first step a suspension of glycerol/water ( $\eta_{liq} = 100$  mPa s) and china clay particles ( $D_{10} \approx 2$   $\mu$ m) was used as non-Newtonian model fluid due to the fact that pure non-Newtonian liquids (e.g. CMC, xanthan gum) may feature in addition to their shear-thinning flow behavior viscoelastic properties which may have an influence on the atomization process. Furthermore, an aqueous solution of carboxymethylcellulose (CMC) was used as pure non-Newtonian liquid without particles. In this case a low molecular weight CMC was chosen to minimize the influence of viscoelasticity. The solutions were mixed for minimum 12 h in a large tank using a special stirrer (cone principle) for gentle mixing. For physical properties refer to Table 2.

**Table 2.** Physical properties of non-Newtonian (NN) model fluids (at 20 °C and 1.013 bar (abs))

	$\eta_{liq,0}$ mPa s	$\eta_{liq,\infty}$ mPa s	$\sigma$ mN m <sup>-1</sup>	$\rho_{liq}$ kg m <sup>-3</sup>	$\mathbf{n} = n + iA$ -	m -	K s
15 wt.% china clay	777	148	64.9	1006	1.450 + i1.000	0.2999	1.20798
2.33 wt.% CMC/H <sub>2</sub> O	420	18	68.9	1325	1.336 + i0.026	0.6297	0.00602

The dynamic viscosity was measured in a rheometer with cylinder measuring system (Searle-type). In case of the NN-fluids the shear viscosity was measured within shear rates of  $\dot{\gamma} = 1 - 4000$  s<sup>-1</sup>. In order to extrapolate the measured shear viscosities to higher shear rates as well as to determine  $\eta_{liq,0} = \eta_{liq}(\dot{\gamma} \rightarrow 0)$  and  $\eta_{liq,\infty} = \eta_{liq}(\dot{\gamma} \rightarrow \infty)$  different power law models from relevant literature were used. For the suspension the data were seen to be well represented by the Carreau-model proposed by Carreau [16]

$$\eta_{liq} = (\eta_{liq,0} - \eta_{liq,\infty})(1 + (K\dot{\gamma})^2)^{-m} + \eta_{liq,\infty} \quad (5)$$

and in case of the CMC/water solution by the Cross-model which was proposed by Cross [17]

$$\eta_{liq} = (\eta_{liq,0} - \eta_{liq,\infty})(1 + (K\dot{\gamma})^m)^{-1} + \eta_{liq,\infty} \quad (6)$$

Surface tension  $\sigma$  and liquid density  $\rho_{liq}$  were measured with a tensiometer applying the Du Noüy ring method and the weighing method for liquid density. The uncertainty of rheometer and tensiometer measurements were estimated using deionized water (surface tension and liquid density) and silicon oil (N) with defined  $\eta_{liq}$ . The uncertainty of the rheometer is below 5 %. For surface tension measurement and liquid density measurement the uncertainty is below 2 % for  $\sigma$  and below 1 % in case of  $\rho_{liq}$ .

Based on laser diffraction spectrometry (LDS) an integral volumetric drop size distribution was measured within the intersection volume of the spray cone and the laser beam line (see Figure 1(a)). All measurements were taken at an axial distance from the nozzle orifice of  $z = 200$  mm. This measuring position was chosen based on two

criteria: First: LDS measurements at various axial positions of the nozzle exit have shown that secondary breakup is completed at approximately  $z = 200$  mm downstream of the nozzle exit, even for the high viscous fluids. Second: High-speed images at  $z = 200$  mm revealed that almost all droplets are spherical for all operating conditions. This aspect is of importance as Pollack and Cuzzi [18] have shown that non-spherical droplets will falsify the measured droplet size distribution obtained with a LDS. The system is equipped with a HeNe-Laser with 632.8 nm wavelength and 10 mm beam diameter. Due to the expected larger droplet sizes of the high viscous sprays a receiver lens with 750 mm focal length was used. This setup allows for nominal droplet size measurements in the range of  $1 \mu\text{m}$  to  $2000 \mu\text{m}$ . For all measurements the Mie-theory (refer to Hergert and Wriedt [19]) was applied for transforming measured light intensity profiles to a particle size distribution. The complex refractive index  $\mathbf{n} = n + iA$  needed for calculation according to the Mie-theory was taken from DOW chemical company [20]. In the case of glycerol/water-mixtures the attenuation coefficient  $A = 0$ . Regarding the NN-fluids refractive index  $n$  was measured using an Abbe-refractometer. Required extinction coefficients  $A$  in case of semi-transparent fluids (CMC/water-mixture) or opaque fluids (china clay suspension) were measured using visible spectroscopy. For all measurements no multiple light scattering correction algorithm was applied due to the fact that for all operational conditions the ratio of non-diffracted light intensity  $I_0$  to the incident light intensity  $I$  was significantly larger than  $T = I/I_0 = 0.5$  which was proposed by Dodge [21] as threshold value. Diodes affected by beam steering (see Mescher and Walzel [22]) were excluded for calculation of the droplet size distribution. All LDS measurements were repeated at least 3 times. A HG-Cam for qualitative investigation of primary and secondary breakup process was employed. The camera features  $f_{rec} = 3.5$  kHz operation at  $1024 \times 1024 \text{ pix}^2$  resolution and frame rates up to  $f_{rec} = 500$  kHz at reduced resolution. A lens with focal length 105 mm was used to capture primary liquid instabilities in the near nozzle region. Each image has a dimension of  $38(H) \times 49(W) \text{ mm}^2$  with a spatial resolution of  $77 \mu\text{m pix}^{-1}$ . The images were captured by backlight illumination through a diffusive screen with a special lighting setup. An array of 9 high-power light-emitting diodes (LED) with total luminous flux of  $9 \times 4500 \text{ lm}$  was used. The position of single LED within the LED array was optimized for best light spread. Due to the homogeneous light distribution and intensity of the light, very short exposure times  $t_{exp} \sim 3 \mu\text{s}$  could be applied. Therefore, this light setup allows for a sharp representation of the jet disintegration and the spray, too. All experiments in the present study were conducted at atmospheric conditions and constant temperature of  $20^\circ\text{C}$ . The operating conditions for the measurements presented below are shown in Table 3. In all experiments the liquid mass flow was kept constant at  $\dot{m}_{liq} = 10 \text{ kg h}^{-1}$  and the GLR was varied by changing  $\dot{m}_{gas}$ .

**Table 3.** Experimental operating conditions at constant  $\dot{m}_{liq} = 10 \text{ kg h}^{-1}$

GLR -	$\dot{m}_{gas}$ $\text{kg h}^{-1}$	$v_{gas}$ $\text{m s}^{-1}$	$v_{liq}$ $\text{m s}^{-1}$	$Re_{gas}$ -	$We_{aero}$ -
0.40 – 1.25	4.0 – 12.5	48 – 151	0.71 – 0.89	5070 – 15960	80 – 860

## Method

A liquid jet surrounded by a high-speed coaxial gas jet disintegrates into droplets via a series of complex physical phenomena. In general two different stages can be distinguished. As a first step the intact liquid sheet disintegrates via different breakup regimes into fragments, ligaments and droplets. This step, taking place in the near nozzle region, is referred to as primary atomization. These regimes proposed by Faragó and Chigier [23] and Lasheras and Hopfinger [24] are the Rayleigh-type breakup, the Membrane-type breakup and the Fiber-type breakup. Classification according to the three regimes is based on liquid Reynolds number  $Re_{liq} = (v_{liq} \rho_{liq} D_{liq}) / \eta_{liq}$  and aerodynamic Weber number ( $We_{aero}$ ). The liquid elements formed in the primary breakup process disintegrate into small droplets via a further step called secondary breakup (see Pilch and Erdman [25]).

For the above mentioned applications, the Fiber-type breakup at high  $We_{aero}$  is of most practical relevance. As proposed by several authors (e.g. Varga et al. [26], Marmottant and Villermaux [27]), the disintegration of a liquid jet into fine droplets via Fiber-type breakup originates from a primary instability that is characterized by the formation of longitudinal waves at the interface between the gas and the liquid at the nozzle exit. This instability can be classified as Kelvin-Helmholtz (KH)-instability. Starting from this symmetric primary instability the formation of transversal waves (secondary Rayleigh-Taylor (RT)-instability) on the longitudinal wave occurs. This leads to the formation of liquid fibers that shear off the liquid jet which results in droplets at a scale comparable to the thickness of the fibers. Both instabilities (KH and RT) are presented in the high-speed images of Figure 2 (left). The passage frequency  $f_{prim}$  of the primary shear instability (KH-instability) can be predicted by a linear instability analysis and is given by the ratio of convection velocity  $u_c$  to axial wavelength  $\lambda$  Eq. (7) of the surging waves.

$$f_{prim} = \frac{u_c}{\lambda} \quad (7)$$

In gas-assisted atomization ( $v_{gas} \gg v_{liq}$ ) considering generic configurations like plane liquid layer as well as on a coaxial liquid jet the theoretical prediction of most amplified wave length  $\lambda$  was done by several authors solving dispersion relations. First, this was performed by Helmholtz [28] and Kelvin [29] (Kelvin-Helmholtz paradigm) for a sharp velocity discontinuity (vanishing low gas boundary layer thickness  $\delta$ ). Based on this approach from Kelvin and Helmholtz first Rayleigh [30] and later Villermaux [31] (theoretically) as well as Raynal et al. [32] (experimentally) showed that if the velocity profile at the gas-liquid interface is not a sharp discontinuity (relevant for most technical cases), gas boundary layer thickness  $\delta$  must be taken into account for prediction of  $\lambda$ . Therefore, the instability analysis from Helmholtz [28] and Kelvin [29] to predict the most amplified wavelength  $\lambda$  was altered by Marmottant and Villermaux [27]. This analysis is based on the boundary layer thickness  $\delta$  of the fast gas stream. Depending on the Weber number  $We_\delta$  calculated with  $\delta$ , the prediction of  $\lambda$  is applied by two different theories: thin vorticity layer  $We_\delta(\rho_{liq}/\rho_{gas})^{0.5} < 1$  (the Kelvin-Helmholtz limit) and thick vorticity layer  $We_\delta(\rho_{liq}/\rho_{gas})^{0.5} > 1$  (the Rayleigh limit). Due to the operational parameters relevant in the present study the Rayleigh limit is relevant. The most amplified wavelength as well as temporal growth given by the equations (8) and (9) as proposed by Marmottant and Villermaux [27] are

$$\lambda \propto \left( \frac{\rho_{liq}}{\rho_{gas}} \right)^{0.5} \delta \quad (8)$$

and

$$\omega \propto \frac{\rho_{gas} v_{gas}}{\rho_{liq} \delta} \quad (9)$$

The convection velocity  $u_c$  estimated from stress continuity at the gas/liquid interface is given by Bernal and Roshko [33] and Dimotakis [34] as

$$u_c = \frac{\sqrt{\rho_{liq} v_{liq}}}{\sqrt{\rho_{liq}} + \sqrt{\rho_{gas}}} + \frac{\sqrt{\rho_{gas} v_{gas}}}{\sqrt{\rho_{liq}} + \sqrt{\rho_{gas}}} \quad (10)$$

The gas boundary layer thickness  $\delta$ , also referred to as vorticity layer thickness, in the gas stream typically decreases with increasing gas velocity  $v_{gas}$  and can be expressed as a function of the gas Reynolds number  $Re_{gas} = (v_{gas} \rho_{gas} L_c) / \eta_{gas}$  calculated with the gas gap thickness  $s_{gas} = (D_{gas} - D_{liq}) / 2$  as characteristic length scale  $L_c$ :

$$\delta \propto L_c (Re_{gas})^{-0.5} \quad (11)$$

According to Eq. (12)

$$f_{prim} \propto \frac{u_c}{\delta} \left( \frac{\rho_{gas}}{\rho_{liq}} \right)^{0.5} \quad (12)$$

derived from inviscid linear instability analysis (Eq. (8) to (10)), it is clear that for constant density ratio  $\rho_{gas}/\rho_{liq}$  the passage frequency increases with gas velocity ( $f_{prim} \propto v_{gas}^{1.5}$ ) as well as with  $v_{liq}$ . At this point it should be mentioned that equation (12) was determined from theoretical analysis assuming low liquid viscosity and experimentally proven using water as low viscous liquid. Experimental results of the present study using viscous Newtonian liquids revealed that  $f_{prim}$  depends on dynamic liquid viscosity  $\eta_{liq}$ , too (see Figure 3).

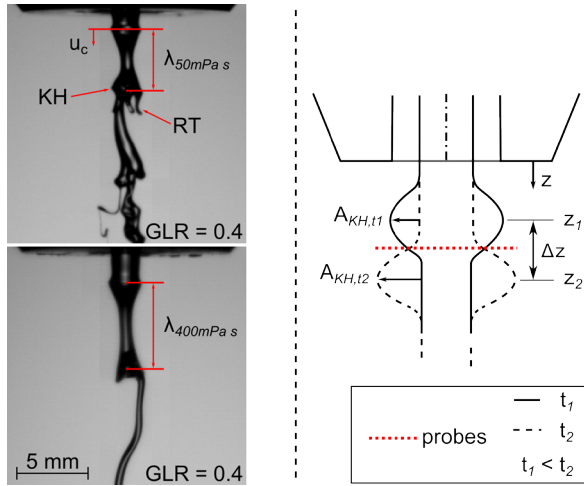


**Figure 2.** HG-cam visualisation of KH- and RT-instability (left) Schema for determination of  $f_{prim}$  and  $u_c$  (right)

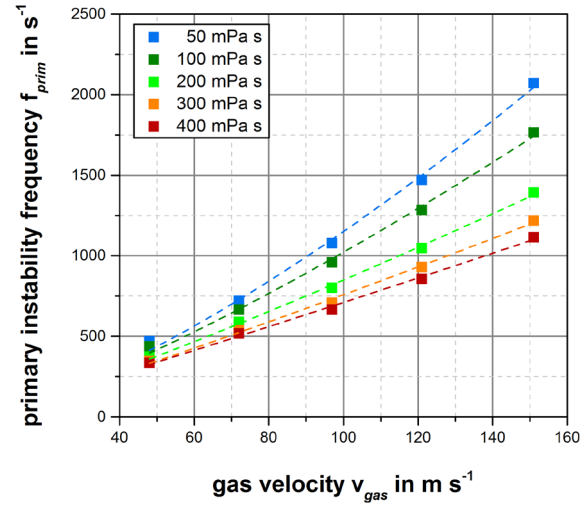


**Figure 3.** Primary instability frequency  $f_{prim}$  for N-fluids as function of  $v_{gas}$  for various  $\eta_{liq}$  at const.  $\dot{m}_{liq} = 10 \text{ kg h}^{-1}$

To measure  $f_{prim}$ , the temporal motion of the longitudinal waves on the liquid surface was captured by a HG-Cam ( $f_{rec} = 12 \text{ kHz}$ ). The resulting time series of digital images were analyzed using an inhouse MATLAB Code (SprayCAT) for image analysis. The passage frequency was measured by an image processing procedure using a threshold detection algorithm for image segmentation proposed by Kapur et al. [35]. A horizontal line of probes (see Figure 2 (right)) detects the existence of liquid at an axial fixed position (pronounced wave amplitude  $A_{KH}$ ) as function of time. This signal was analyzed using a fast Fourier transform algorithm (FFT). The frequency of the most intensified peak from the power spectrum of the FFT was kept as mean passage frequency  $f_{prim}$ . For a high frequency resolution of the FFT, 4000 pictures were analyzed ( $\pm 3 \text{ Hz}$ ). Due to the high  $f_{rec} = 12 \text{ kHz}$  Nyquist stability criterion was always fulfilled. The measured frequencies increases with  $v_{gas}$  and decreases with increasing viscosity  $\eta_{liq}$  (see Figure 3). Based on this dependence of  $f_{prim}$  on  $\eta_{liq}$ , the present study is focused on a new experimental approach to estimate the apparent shear viscosity  $\eta_{liq}^*$  relevant for jet breakup during atomization of a NN-fluids by a co-flowing gas jet. Knowing  $f_{prim} = f(\eta_{liq})$  from experiments atomizing N-fluids enables determination of  $\eta_{liq}^*$  by measuring  $f_{primNN}$  from atomization of NN-fluids, see Figure 4. However, a model based description of  $f_{prim}$  is needed as function of  $\eta_{liq}$  and other relevant parameter as well, see Eq. (13).

$$f_{prim,fit} = f(\eta_{liq}, v_{gas}, v_{liq}, \rho_{gas}, \rho_{liq}) \quad (13)$$

For this purpose, the existing equations (8), (10) and (12) from inviscid linear instability analysis have been extended by additional empirical parameter to take  $\eta_{liq}$  into account. At this point it should be emphasized that within the scope of this study as a first step solely the influence of shear viscosity on primary instability frequency  $f_{prim}$  is considered. Due to the fact that for NN-fluids the ratio of extensional viscosity to shear viscosity is not constant as it is for N-fluids (Trouton's ratio of 3), a possible influence of extensional viscosity on  $f_{prim}$  has to be considered separately as well and will be investigated in further investigations.

First, convection velocity  $u_c$  was determined experimentally by wave front tracking  $u_c \approx \Delta z / t_{rec}$ , see Figure 2 (right). For this purpose the axial distance  $\Delta z$  moved by the wave front within five time steps  $t_{rec} = 5 f_{rec}^{-1}$  was determined using high-speed images, always initiating from the same amplitude height  $A_{KH,t1}$ . The experimentally determined values of  $u_c$  are plotted as function of  $v_{gas}$  for various  $\eta_{liq}$  in Figure 5. As proposed by equation (10) convection velocity increases with  $v_{gas}$  and certainly, according to these values, there is no or just a negligible small dependence of  $u_c$  on  $\eta_{liq}$  at constant  $v_{gas}$  which can be reasoned by the following consideration: The wave front is accelerated by the force resulting from the static pressure of the gas jet. The forces which counteract the force of the gas jet are inertia force  $F_I = A_{cir} \rho_{liq} a$  and viscous force  $F_\eta = \eta_{liq} A_{lat} \partial v / \partial x$  of the liquid. The value  $a$  defines acceleration and  $A_{cir}$ ,  $A_{lat}$  and  $s$  correspond to the cross sectional area, the lateral surface area as well as to an axial ( $z$ -direction) length scale of the free liquid jet. Due to the fact that  $\dot{\gamma} = \partial v_{liq} / \partial x$  is probably much lower for the considered case (free liquid surface) compared to no-slip conditions at a solid boundary (e.g. tube flow  $\dot{\gamma}_{inj} = 8 v_{liq} / D_{liq}$ ) resistance based on  $F_I$  is larger compared to  $F_\eta$ . This was proven calculating the ratio  $F_\eta / F_I$  for several discrete volume element  $dV = A_{cir} dz$  of the liquid column as function of time using experimental difficult accessible data ( $a$  and  $\partial v_{liq} / \partial x$ ) from Volume-of-Fluid simulation (VoF) of the experiment under consideration. This estimate revealed that even for  $\eta_{liq} = 400 \text{ mPa s}$  the average of  $F_I$  is about one order of magnitude higher than  $F_\eta$ . In addition, at constant gas velocity  $F_I$  is nearly independent from the selected fluid

( $\eta_{liq} = 50 - 400 \text{ mPa s}$ ) due to nearly constant  $\rho_{liq}$  (see Table 1). Therefore, within this work  $u_c$  is considered as independent of  $\eta_{liq}$ . Solely, for determination of  $u_{c,fit}$  the slope of Eq. (10) was adjusted to the measured values by a prefactor  $C_1$ .

Determination of wave length  $\lambda$  from high-speed cam data (see Figure 2 (left)) as well as from calculation  $\lambda_{exp} = u_{c,exp}/f_{prim,exp}$  (see Figure 6) revealed that  $\lambda$  depends apart from  $v_{gas}$  on  $\eta_{liq}$ , too.

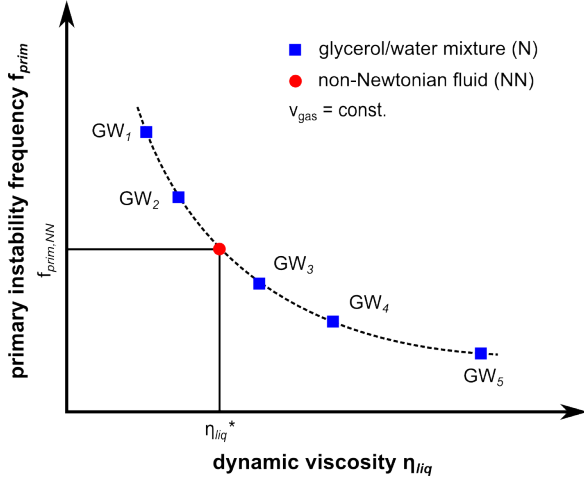


**Figure 4.** Schema for determination of apparent liquid viscosity  $\eta_{liq}^*$  using primary instability analysis

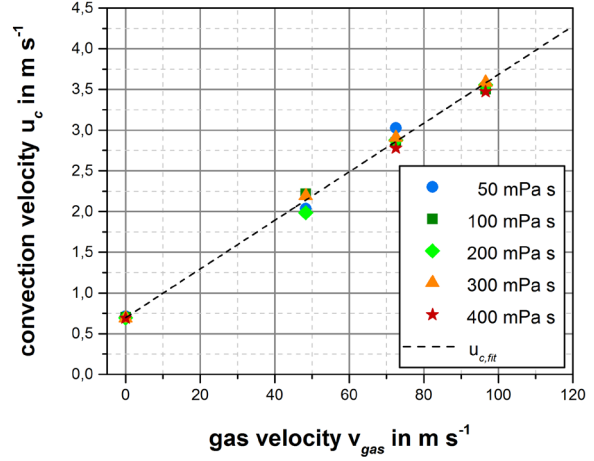


**Figure 5.** Influence of convection velocity  $u_c$  on  $v_{gas}$  for various  $\eta_{liq}$  at const.  $\dot{m}_{liq} = 10 \text{ kg h}^{-1}$  (N-fluids)

As shown in Figure 6 experimental values of wave length  $\lambda$  (points with dashed line) decrease with  $v_{gas}$  as proposed by inviscid instability analysis and increase with  $\eta_{liq}$ . Viscosity dampens the growth of disturbances and therefore reduces the growth rate  $\omega$  of the longitudinal wave (KH-instability) considered in this study. The influence of liquid viscosity on growth rate and wave length has been studied in literature solely for liquid sheets (e.g. flat fan nozzle) and non-gas assisted atomization (e.g. single fluid nozzle). However, the authors revealed the same influence of liquid viscosity on wave length  $\lambda$  or respectively on wave number  $k = 2\pi/\lambda$  presented in the form of dispersion relation diagrams, e.g. Cousin and Dumouchel [36]. In order to consider the influence of  $\eta_{liq}$  on  $\lambda$  equation (8) has been extended by the parameter  $C_\eta$  to

$$\lambda_{fit} = C_\eta \left( \frac{\rho_{liq}}{\rho_{gas}} \right)^{0.5} \delta. \quad (14)$$

This parameter is determined by the least square method for each liquid viscosity experiment ( $\eta_{liq} = 50 - 400 \text{ mPa s}$ ) and can be expressed as function of Ohnesorge number in terms of a power law according to  $C_\eta \propto Oh^{0.194}$ . Comparing  $\lambda_{fit}$  with experimentally measured wave lengths (see Figure 6) depicts good agreement at low liquid viscosity but shows increasing discrepancies between measured and fitted values with increasing  $\eta_{liq}$ . The model based values for  $f_{prim,fit}$  are calculated by the ratio of  $u_{c,fit}$  and  $\lambda_{fit}$ . In Figure 7 the correlation between the experimental  $f_{prim,exp}$  and calculated values  $f_{prim,fit}$  of the passage frequencies are shown. The plot depicts a maximum deviation of 16.3 % in the large gas velocity range and 10.2 % in the low region which may be considered as not too bad but is not acceptable for the purpose to determine the apparent viscosity  $\eta_{liq}^*$ .

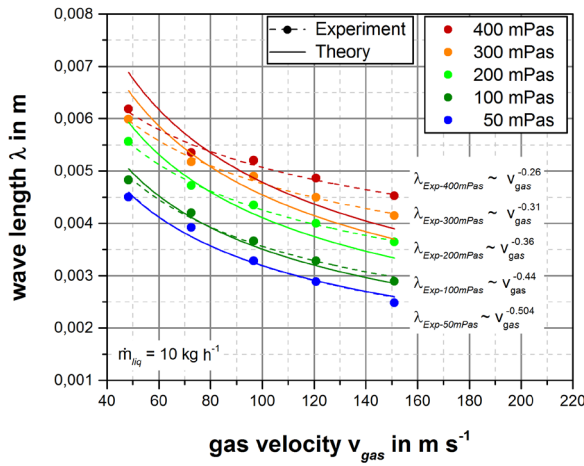


**Figure 6.** Wave length versus  $v_{gas}$  for various  $\eta_{liq}$  (N-fluids); Fit data belongs to model  $\lambda_{fit}$  with  $\beta \neq f(\eta_{liq})$

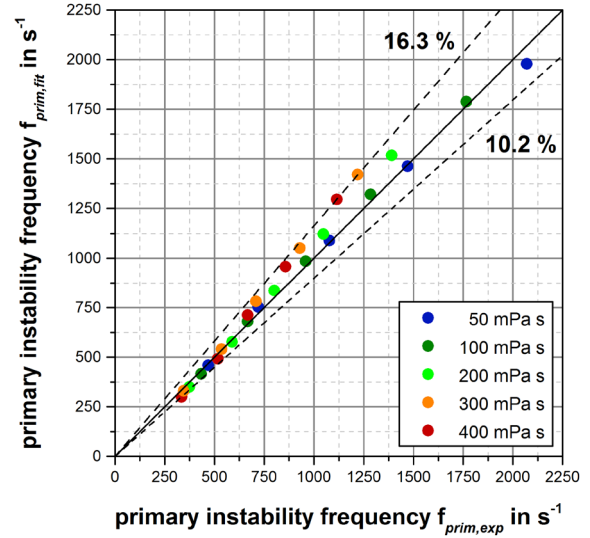


**Figure 7.** Predicted  $f_{prim,fit}$  for  $\beta \neq f(\eta_{liq})$  as function of measured  $f_{prim,exp}$  at relevant operating conditions (N-fluids)

As can be seen from Figure 3, particularly at low gas velocity the dependence of  $\eta_{liq}$  on  $f_{prim}$  is weak. This means that minor deviations of  $f_{prim,fit}$  result in large deviations from corresponding  $\eta_{liq}$ . Therefore, to achieve a more precise model based description of  $\lambda_{fit}$  and  $f_{prim,fit}$ , respectively, in a first attempt an additional empirical correction factor has been included in Eq. (14) which is described in the following: At this point it is important to mention that gas boundary layer thickness  $\delta$  is a key parameter controlling the instabilities at the gas to liquid interface. According to theory from Marmottant and Villermaux [27] (see Eq. (8) and (11))  $\lambda$  is directly proportional to the boundary layer thickness  $\delta$  which is proportional to  $v_{gas}^{-0.5}$ . Scaling of  $\delta$  with  $v_{gas}^\beta$  involving  $\beta = -0.5$  according to theory is strictly valid for laminar flow conditions. In case of turbulent flow conditions the scaling parameter  $\beta$  is defined by  $\beta \approx -0.2$  according to literature (e.g. Schlichting and Gersten [37]). Therefore, for transition from laminar flow to turbulent flow  $\beta$  is somewhere in between  $\beta \in [-0.5, -0.2]$ . The evolution of  $\lambda$  with gas velocity for various  $\eta_{liq}$  is reported in Figure 6. At low viscosity ( $\eta_{liq} = 50$  mPa s)  $\lambda$  scales with  $\beta \approx -0.5$  as expected from equation (8) and (11). In contrast, with increasing liquid viscosity  $\lambda$  scales no longer with  $\beta = -0.5$ . As can be seen from experimental data the scaling exponent  $\beta$  increases with  $\eta_{liq}$ . The explanation for this effect might be a change in evolution of boundary layer thickness with increasing  $\eta_{liq}$ . However, based on the damping influence of viscosity on growth rate, the axial position where the wave emerges from the undisturbed liquid surface is shifted towards longer distances downstream the nozzle exit with increasing  $\eta_{liq}$ . This could affect  $\delta$  at this position due to the fact that transition from laminar to turbulent conditions depends not only on  $v_{gas}$  but also on flow distance ( $L_c$ ). The fact that evolution of  $\lambda$  with  $v_{gas}$  for the lowest viscosity ( $\eta_{liq} = 50$  mPa s) scales with  $\beta \approx -0.5$  supports this theory as it is proven experimentally for water that  $\lambda$  scales with  $v_{gas}^{-0.5}$  by several authors (e.g. Marmottant and Villermaux [27], Raynal et al. [32]). Furthermore, with increasing viscosity a slight tapering of the liquid jet with increasing downstream distance can be observed. This could affect the gas boundary layer thickness because the liquid surface is not parallel to the gas jet and therefore  $\delta$  increases. As a consequence the evolution of wave length  $\lambda$  is affected as well. A similar effect on  $\delta$  and therefore on  $\lambda$  through thinning of the liquid jet in the near nozzle region was noted by Marmottant and Villermaux [27] due to pronounced influence of gravity at low liquid velocity.

In order to take account of the influence of  $\eta_{liq}$  on the evolution of  $\delta$  the scaling parameter  $\beta$  is no longer constant but rather is expressed as function of Oh in terms of a power law according to  $\beta \propto Oh^{-0.316}$ . Finally, the model based description of  $\lambda_{fit}$  is expressed with  $C_\eta \propto Oh^{-0.905}$  according to equation (15).

$$\lambda_{fit} = C_\eta \left( \frac{\rho_{liq}}{\rho_{gas}} \right)^{0.5} L_c \left( \frac{v_{gas} L_c \rho_{gas}}{\eta_{gas}} \right)^\beta \quad (15)$$

Comparing experimental data with calculated data from equation (15) (Figure 8) shows good agreement for all considered viscosities. In addition, in Figure 9 correlation between the experimental and calculated values of the passage frequencies  $f_{prim,fit} = u_{c,fit}/\lambda_{fit}$  are shown. High quality of model based description is confirmed by the correlation coefficient  $R^2 \approx 1$ . This correlation, based on inviscid linear instability analysis of longitudinal KH-wave, provides the basis to estimate the apparent viscosity relevant for jet breakup atomizing non-Newtonian fluids using EMTFA. Thus measuring  $f_{prim,NN}$  by atomizing NN-fluids, the apparent viscosity  $\eta_{liq}^*$  can be deduced from

the extended model  $\eta_{liq}^* = f(f_{prim,NN}, v_{gas}, v_{liq}, \rho_{gas}, \rho_{liq})$ . The applicability of this method is tested and evaluated using two different NN-fluids within the next section.

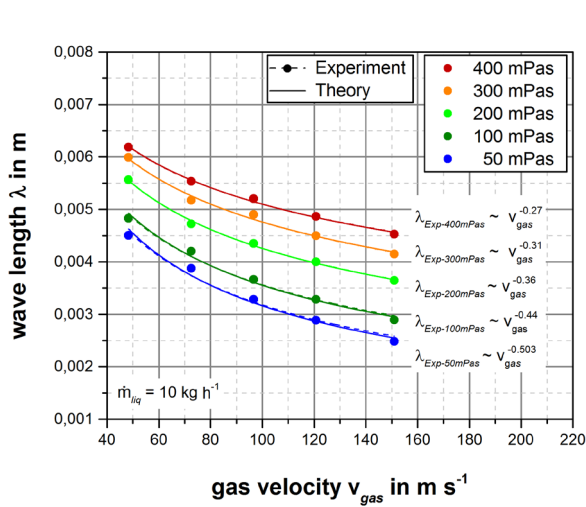


**Figure 8.** Wave length versus  $v_{gas}$  for various  $\eta_{liq}$  (N-fluids); Fit data belongs to model  $\lambda_{fit}$  with  $\beta = f(\eta_{liq})$

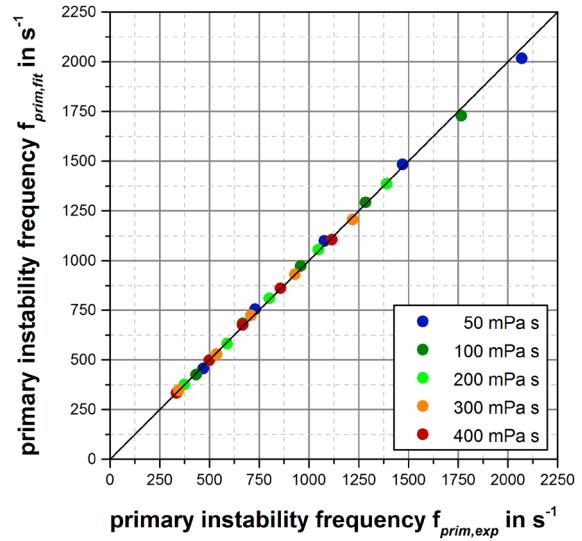


**Figure 9.** Predicted  $f_{prim,fit}$  for  $\beta = f(\eta_{liq})$  as function of measured  $f_{prim,exp}$  at relevant operating conditions (N-fluids)

## Results and discussion

In order to check the applicability of the new method for determination of apparent viscosity  $\eta_{liq}^*$  as a first step a suspension consisting of a glycerol/water-mixture with  $\eta_{liq} = 100$  mPa s (continuous phase) with suspended china clay particles (disperse phase) was used as model fluid. Suspensions of this type exhibit a distinct shear-thinning flow behavior due to the edged particle shape of the china clay particles. Such a suspension is particularly suitable for two reasons: Shear-thinning suspensions of this type with a Newtonian continuous phase exhibit comparatively less viscoelastic properties as compared to pure non-Newtonian liquids due to the fact that shear-thinning can be attributed to the edged particle shape of the china clay particles and not due to coiled long molecular chains which typically cause viscoelasticity of pure NN-liquids. This consideration is important due to the fact that the possible influence of extensional viscosity is preliminary not considered for model based description of  $f_{prim,NN}$ . Furthermore, with the use of a continuous phase with uniquely defined liquid viscosity the estimated apparent viscosity must be above this threshold value ( $\eta_{liq}^* \geq 100$  mPa s).

The effect of shear-thinning flow behavior on jet disintegration and spray formation is qualitatively shown in Figure 10 using high-speed images. The jet disintegration of the non-Newtonian suspension ( $x_{cc} = 15$  wt.%) with  $\eta_{liq,0} = 777$  mPa s is shown in Figure 10 (b) and can be compared with the jet disintegration of a pure Newtonian fluid (glycerol/water-mixture) with  $\eta_{liq} = 400$  mPa s, see Figure 10 (a). Gas velocity ( $v_{gas} = 97$  m s<sup>-1</sup>) and mass flow of liquid ( $\dot{m}_{liq} = 10$  kg h<sup>-1</sup>) were kept constant (GLR = 0.8).

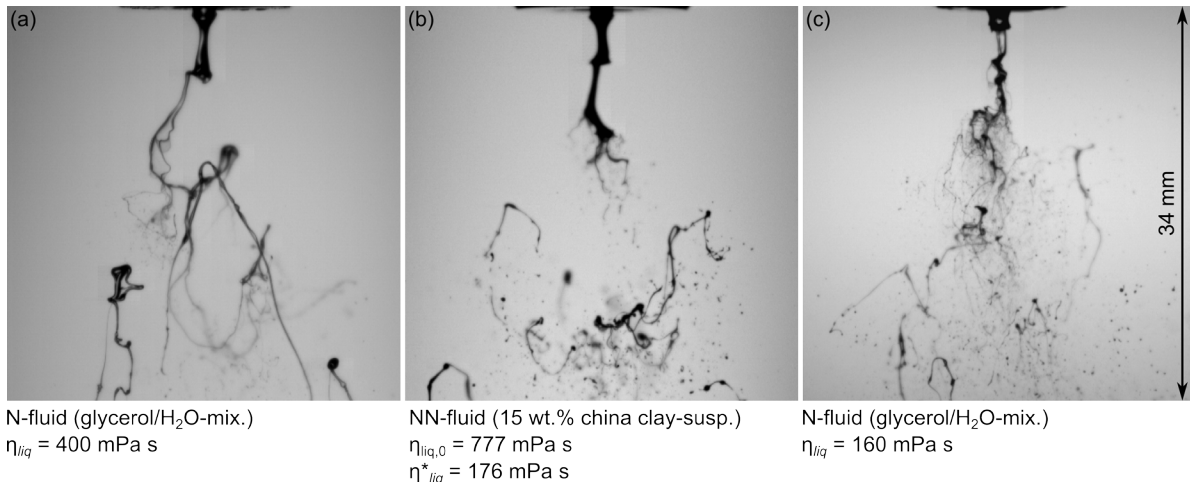


**Figure 10.** High-speed visualization of jet breakup for two N-fluids (a)(c) and one NN-fluid (b) ( $v_{gas} = 97$  m s<sup>-1</sup>)

A significantly different breakup behavior can be observed for Figure 10 (a) and (b). Even though zero viscosity  $\eta_{liq,0} = \eta_{liq}(\dot{\gamma} \rightarrow 0)$  of the NN-fluid is significantly higher as compared to the N-fluid ( $\eta_{liq,0} = 777 \text{ mPa s} \gg \eta_{liq} = 400 \text{ mPa s}$ ), jet breakup of the NN-fluid indicates shorter disintegration lengths and times as compared to the N-fluid. Obviously more droplets and fewer ligaments can be seen on image in Figure 10 (b) as compared to image in Figure 10 (a). This may be attributed to the lower actual viscosity of the shear-thinning fluid due to shear between gas and liquid phase at the nozzle exit. In fact, the determination of the apparent viscosity  $\eta_{liq}^*$  by the use of the new method described above revealed a significantly lower apparent viscosity for the NN-suspension. From the measured primary instability frequency  $f_{prim,NN} = 785 \text{ Hz}$  of the suspension at  $v_{gas} = 97 \text{ m s}^{-1}$  the apparent viscosity is determined to  $\eta_{liq}^* = 176 \text{ mPa s}$ . This value is considerably lower compared to  $\eta_{liq,0} = 777 \text{ mPa s}$ . Thus, the effect of shear-thinning on jet breakup due to interaction between liquid- and gas-phase can be confirmed. Comparison of the jet breakup in Figure 10 (b) with a N-fluid similar in viscosity, see Figure 10 (c), reveals comparable jet breakup phenomena regarding size and length of the ligaments as well as number of droplets visible. In addition, determination of  $f_{prim}$  for gas velocities in the range of  $48 \text{ m s}^{-1}$  to  $180 \text{ m s}^{-1}$  revealed that the apparent viscosity  $\eta_{liq}^*$  decreases with increasing  $v_{gas}$  (starting from  $\eta_{liq}^*(48 \text{ m s}^{-1}) = 190 \text{ mPa s}$ ) and approaches asymptotically a threshold viscosity value in the range of  $140 \text{ mPa s} < \eta_{liq}^* < 160 \text{ mPa s}$ . It is worth mentioning that this value is within the range expected ( $\eta_{liq,\infty} = 148 \text{ mPa s}$ , see Table 2) and above the limiting viscosity value  $\eta_{liq} = 100 \text{ mPa s}$  of the continuous phase (glycerol/water-mixture) which supports the functionality of the method.

Furthermore, in a first attempt the new method for determination of apparent viscosity was tested to correlate spray quality ( $ID_{32}$ ) with the extended Ohnesorge number  $Oh^*$  (Eq. (4)). Therefore, an existing model for prediction of drop size ( $ID_{32}$ ) for the atomization of N-liquids (glycerol/water-mixtures) within a large range of viscosities ( $\eta_{liq} = 50 - 400 \text{ mPa s}$ ) was used. Based on the correlation of Mulhem et al. [6] the drop size is expressed in terms of three dimensionless numbers  $Oh$ ,  $GLR$  and  $We_{aero}$ :

$$ID_{32} = C D_{liq} Oh^m (GLR We_{aero})^n \quad \begin{array}{l} C = 5.462 \cdot 10^6 \\ m = 0.136 \\ n = -0.809 \end{array} \quad (16)$$

The exponents  $m$  and  $n$  as well as the coefficient  $C$  were determined by least-square method to fit the experimental results from LDS measurements at  $x = 0 \text{ mm}$ ,  $y = 0 \text{ mm}$  and  $z = 200 \text{ mm}$  (the physical unit of  $D_{liq}$  is meter). In this case the used NN-liquid (CMC/water-mixture) was atomized at operating conditions mentioned above, see Table 3. Both, drop size  $ID_{32}$  (LDS) as well as  $f_{prim,NN}$  (HG-Cam) were determined experimentally. Again, concentration of CMC was kept low to minimize the influence of viscoelasticity. Based on the measured primary instability frequencies  $f_{prim,NN}$  the apparent viscosity  $\eta_{liq}^*$  (see Figure 11) was determined for this fluid by the use of the new method as well. As shown in Figure 11,  $\eta_{liq}^*$  decreases with  $v_{gas}$ , which can be attributed to increasing shear within the liquid jet due to increasing aerodynamic forces. By the use of those spray data within a next step it was proven whether it is appropriate to estimate the  $ID_{32}$  data from atomization of the CMC/water-mixture applying equation (16) by the use of  $\eta_{liq,0}$ ,  $\eta_{liq,\infty}$  or  $\eta_{liq}^*$ . Therefore, in Figure 12 the Sauter mean diameter predicted by the model  $ID_{32,fit}$  (see Eq. (16)) is plotted against the Sauter mean diameter obtained from the atomization experiment  $ID_{32,exp}$ . Three different definitions of the extended Ohnesorge number

$Oh^* = \eta_{liq,0} | \eta_{liq,\infty} | \eta_{liq}^* / (\sigma \rho_{liq} D_{liq})$  are used. As a result the coefficient of determination  $R^2$  emphasizes that the use of the apparent viscosity  $\eta_{liq}^*$  within the model based description (Eq. (16)) is most appropriate for modeling the measured spray data of the NN CMC/water-mixture. By the use of  $\eta_{liq,\infty}$  the experimental values are obviously underestimated. This is due to fact that  $\eta_{liq,\infty}$  is much lower compared to the determined  $\eta_{liq}^*$  values, even at high gas velocities. The deviation between experimental and fitted values is lower in case of  $\eta_{liq,0}$  but still present.

Based on these preliminary qualitative as well as quantitative investigations, the use of  $\eta_{liq}^*$  for determination of the extended Ohnesorge number is indeed the most appropriate choice to correlate spray data ( $ID_{32}$ ) as well as to characterize primary breakup morphology.

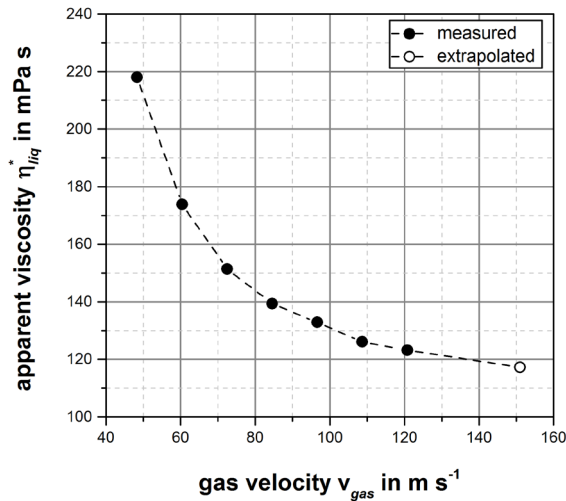


**Figure 11.** Influence of  $\eta_{liq}^*$  on gas  $v_{gas}$ ;  
Fluid: (NN) 2.33 wt.% CMC/H<sub>2</sub>O-mixture

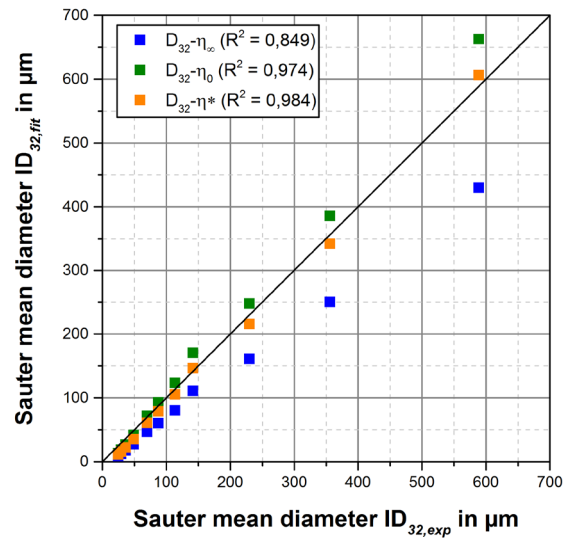


**Figure 12.**  $ID_{32,fit}$  vs.  $ID_{32,exp}$  for various definition of  $Oh^*$ ;  
Fluid: (NN) 2.33 wt.% CMC/H<sub>2</sub>O-mixture

## Conclusions

Motivated by the atomization of non-Newtonian fluids in industrial applications, the research work of the present study was focused on a new experimental approach to estimate the apparent shear viscosity  $\eta_{liq}^*$  at the jet breakup process using an EMTFA. The relevant results from this study are summarized in the following:

- The experimental approach is based on the viscosity dependence of the passage frequency  $f_{prim}$  of shear instability (Kelvin-Helmholtz type) in the near nozzle region ( $f_{prim} \downarrow$  with  $\eta_{liq} \uparrow$ ). Knowing  $f_{prim}$  as function of  $\eta_{liq}$  the apparent viscosity  $\eta_{liq}^*$  can be deduced from measuring  $f_{prim,NN}$  during atomization of NN-fluids.
- It was shown qualitatively that the shear-thinning effect favors primary jet disintegration (i.e. less ligaments, more droplets) compared to a pure N-fluid. The assumption that the viscosity of the liquid jet is lowered by the shear rates at the nozzle exit was confirmed by the new method.
- For both investigated NN-fluids a dependence of  $\eta_{liq}^*$  from  $v_{gas}$  was shown ( $\eta_{liq}^* \downarrow$  with  $v_{gas} \uparrow$ ). This can be explained by the fact that increase in  $v_{gas}$  results in increase of  $\dot{\gamma}$ . For the operating conditions under consideration the liquid is sheared to a viscosity value intermediate between  $\eta_{liq,0}$  and  $\eta_{liq,\infty}$  during jet breakup. The dependence of  $\eta_{liq}^*$  on  $v_{gas}$  is more pronounced for low gas velocities.
- A first attempt to correlate spray quality in terms of  $ID_{32}$  with an extended Ohnesorge number  $Oh^*$  by the use of  $\eta_{liq}^*$  determined with the new method was successful. The accuracy of the model ( $ID_{32,fit}$  vs.  $ID_{32,exp}$ ) increases by the use of  $\eta_{liq}^*$  instead of  $\eta_{liq,0}$  or  $\eta_{liq,\infty}$  as it is common in literature.

Finally, the results presented here show that it is possible making prediction of spray quality for a certain nozzle solely from measuring  $f_{prim}$  under the premise of onetime determination of  $f_{prim}$  as function of  $\eta_{liq}$ . This fact will contribute to optimize and control the operation of gas-assisted atomizers with non-Newtonian fluids by simple high-speed camera measurements (e.g. operation of EFG with low grade fuels with time and feedstock sensitive fluid viscosity). Nevertheless, the applicability and accuracy of the new method must be investigated by the use of further non-Newtonian fluids with different rheological properties. Therefore, the possible influence of extensional viscosity on primary instability frequency, which was initially not considered in this study, has to be considered within the model based description of  $f_{prim,fit}$  as well. The influence of extensional viscosity on primary instability frequency could be investigated separately by the use of different non-Newtonian liquids featuring similar flow curves (viscosity vs. shear rate) but different extensional viscosities, for example.

## Acknowledgements

The authors would like to thank the Helmholtz Association of German Research Centres (HGF) for funding. A special thank goes to Thomas Müller from KIT Engler-Bunte-Institute (division combustion technology) for providing Volume of Fluid (VoF) data.

## References

- [1] Higman, C., and van der Burgt, M., 2008, "Gasification, 2nd Edition". Gulf Professional Publishing.
- [2] Hede, P. D., Bach, P., and Jensen, A. D., 2008, Chemical Engineering Science, 63, pp. 3821-3842.
- [3] Kolb, T., and Eberhard, M., Nov. 19.-21. 2013, IEA Bioenergy 2nd Semi-Annual Task Meeting 'Task 33'.

- [4] Sänger, A., Jakobs, T., Djordjevic, N., and Kolb, T., Sep. 8.-10. 2014, 26th European Conference on Liquid Atomization and Spray Systems.
- [5] Kim, K. Y., and Marshall, W. R., 1971, *AICHE Journal*, 17, pp. 575-584.
- [6] Mulhem, B., Bauckhage, K., Fritsching, U., and Schulte, G., July 13.-17. 2003, 9th International Conference on Liquid Atomization and Spray Systems.
- [7] Schmelz, F., and Walzel, P., 2003, *Chemie Ingenieur Technik*, 75, pp. 200-207.
- [8] Aliseda, A., Hopfinger, E. J., Lasheras, J. C., Kremer, D. M., Berchielli, A., and Connolly, E. K., 2008, *International Journal of Multiphase Flow*, 34, pp. 161-175.
- [9] Mansour, A., and Chigier, N., 1995, *Journal of non-Newtonian Fluid Mechanics*, 58, pp. 161-194.
- [10] Gillberg, L., Larsson, N., Mathiesen, M., Nyström, O., and Persson, J., 1983, "Some Rheological Data and Atomization Behaviour of CWM's Containing 68 to 89 % Coal", Technical report AB Carbogel, Helsingborg, Sweden.
- [11] Zhao, H., Liu, H., Xu, J., Li, W., and Cheng, W., 2012, *Chemical Engineering Science*, 78, pp. 63-74.
- [12] Maurer, A., 2002, "Grundlagen und experimentelle Untersuchungen zum Zerstäuben von Druckfarben zur Farbdosierung bei Offsetfarbwerken", Ph.D. thesis, <http://monarch.qucosa.de/fileadmin/data/qucosa/documents/4647/data/dissertation-andreas-maurer-17-dez-2002.pdf>
- [13] Buckner, H., and Sojka, P., 1993, *Atomization and Sprays*, 3, pp. 157-170.
- [14] Kampen, J., Ciezki, H., Tiedt, T., and Madlener, K., 2006, "Some Aspects of the Atomization Behavior of Newtonian and of Shear-thinning Gelled non-Newtonian Fluids with an Impinging Jet Injector", Technical report DLR, Hardthausen, Germany, [http://www.raumfahrtantriebe.de/spray2006/files/spray06\\_ciezki\\_final\\_paper.pdf](http://www.raumfahrtantriebe.de/spray2006/files/spray06_ciezki_final_paper.pdf)
- [15] Meier, G., Klöpffer, A., and Grabitz, G., 1992, *Experiments in Fluids*, 12, pp. 173-180.
- [16] Carreau, P. T., 1972, *Transactions of the Society of Rheology*, 16, pp. 99-127.
- [17] Cross, M.M., 1965, *Journal of Colloid Science*, 20, pp. 417-437.
- [18] Schuerman, D., 1980, "Light Scattering by Irregularly Shaped Particles", Plenum Press, New York, Chap. 4.
- [19] Hergert, W., and Wriedt, T., 2012. "The Mie Theory". Springer.
- [20] DOW Chemical, "Refractive Index of Glycerine-Water Solutions at 20 °C", [http://msdssearch.dow.com/PublishedLiteratureDOWCOM/dh\\_0032/0901b803800322b7.pdf?filepath=glycerine/pdfs/noreg/115-00667.pdf&fromPage=GetDoc.](http://msdssearch.dow.com/PublishedLiteratureDOWCOM/dh_0032/0901b803800322b7.pdf?filepath=glycerine/pdfs/noreg/115-00667.pdf&fromPage=GetDoc.) ([cit. 2014-02-01]).
- [21] Dodge, L. G., 1984, *Optical Engineering*, 23, pp. 626-630.
- [22] Mescher, A., and Walzel, P., 2010, *Chemie Ingenieur Technik*, 82, pp. 717-722.
- [23] Faragó, Z., and Chigier, N., 1992, *Atomization and Sprays*, 2, pp. 137-153.
- [24] Lasheras, J. C., and Hopfinger, E.J., 2000, *Annual Review of Fluid Mechanics*, 32, pp. 275-308.
- [25] Pilch, M., and Erdman, C.A., 1987, *Int. Journal of Multiphase Flow*, 13, pp. 741-757.
- [26] Varga, C. M., Lasheras, J. C., and Hopfinger, E. J., 2003, *Journal of Fluid Mechanics*, 497, pp. 405-434.
- [27] Marmottant, P., and Villermaux, E., 2004, *Journal of Fluid Mechanics*, 498, pp. 73-111.
- [28] Helmholtz, H., 1868, *Philosophical Magazine*, 36, pp. 337-346.
- [29] Kelvin, W.T., 1871, *Philosophical Magazine*, 42, pp. 362-377.
- [30] Rayleigh, Lord, 1880, *Proceedings of the London Mathematical Society*, 11, pp- 57-72.
- [31] Villermaux, E., 1998, *Journal of Propulsion and Power*, 14, pp. 807-817.
- [32] Raynal, L., Villermaux, E., Lasheras, J., and Hopfinger, E., 1997, 11th International Symposium on Turbulent Shear Flows, 3, pp. 27.1-27.5.
- [33] Bernal, L., and Roshko, A., 1986, *Journal of Fluid Mechanics*, 170, pp. 499-525.
- [34] Dimotakis, P., 1986, *The American Institute of Aeronautics and Astronautics*, 24, pp. 1791-1796.
- [35] Kapur, N., Sahoo, P.K., and Wong, A., 1985, *Computer Vision, Graphic, Image Processing*, 29, pp. 273-285.
- [36] Cousin, J., and Dumouchel, C., 1996, *Atomization and Sprays*, 6, pp. 563-576.
- [37] Schlichting, H., and Gersten, K., 2000, "Boundary-Layer Theory". Springer.